

<https://doi.org/10.1038/s41612-025-01021-z>

# Growing human-induced climate change fingerprint in regional weekly fire extremes

Sifang Feng<sup>1,2</sup>✉, Jakob Zscheischler<sup>1,3</sup>, Zengchao Hao<sup>2</sup> & Emanuele Bevacqua<sup>1</sup>✉

Wildfires cause large damage to natural and human systems. Despite the clear connection between human-induced climate change and increased fire weather risk, a global, systematic attribution of observed extreme fires to human-induced climate change is lacking. Here, we address this gap by first linking observed regional weekly burned area extremes (>85th percentile) to the fire weather index (FWI) during the fire seasons of 2002–2015 via a logistic regression model, and then using simulations from climate models to quantify the impact of human-induced climate change. Focusing on regions with good predictability of the statistical model, we find that human-induced climate change was responsible for a fraction equal to 8% ( $\pm 4\%$ , standard deviation across climate models) of the predicted probability of more than 700 regional fire extremes on average, thereby increasing the probability of experiencing a fire extreme across 15 out of 19 analysed regions. While higher temperature is the main driver of the increased fire extreme probability, shifts in precipitation, relative humidity, and/or wind speed substantially modulated fire changes across many regions. Mainly because of warming, the probability of extreme fires attributable to human-induced climate change increased by 5.2%/decade globally over 2002–2015, in line with an acceleration of the climate-driven enhancement of fire extremes over the last decades that may continue in the near future. These findings highlight the urgent need for sustainable fire management strategies.

Fires can pose large threats to socioeconomic and environmental systems throughout the world<sup>1–3</sup>. Globally, they contribute to about 25% of the world's forest losses annually<sup>4</sup> and endanger at least 15% of the terrestrial and freshwater species, according to the International Union for the Conservation of Nature (IUCN)<sup>5</sup>. Fires result in 8 billion tonnes of CO<sub>2</sub> emissions in the atmosphere<sup>6</sup> and are responsible for 5–8% of the 3.3 million premature deaths due to air quality issues every year<sup>1</sup>. While global observed burned areas decreased due to agricultural expansion and intensification over the last decades<sup>7</sup>, fire-conducive weather, characterised by dry, hot, and wind conditions, has increased over the recent decades<sup>8,9</sup> and is projected to increase further in the future<sup>10</sup>. In view of possible shifts in several meteorological drivers of fires<sup>10</sup> due to the changing climate, quantifying the effect of human-induced climate change on extreme fire events has become a priority in developing effective mitigation strategies and reducing fire risks.

Existing attribution studies predominantly link individual fire events to climate change by examining changes in the fire-prone weather. Most regional studies have quantified the human-induced

climate change effect on the change in the Fire Weather Index (FWI), an index that integrates multiple meteorological drivers of fires, including precipitation, temperature, relative humidity, and wind speed. For instance, recent studies focussed on the near-record-breaking 2003 fire in France<sup>11</sup>, the 2018 forest fire in Sweden<sup>12</sup>, and the 2019–2020 Australian bushfires<sup>13</sup>. While informative, these regional studies do not provide a systematic perspective on the effect of human-induced climate change on the multiple fires that have occurred worldwide. Furthermore, the contribution of human-induced climate change on fire-conducive weather conditions does not represent that on fire itself, given that the effects of weather on fires are not directly proportional to meteorological conditions<sup>14</sup>. Thus, even global attribution studies focusing on observed change in FWI also provide only partial insights into climate change effects on fires<sup>10,15</sup>. Attributing actual fire activity to climate change is more challenging than attributing meteorological events because the former requires linking climate change's effect on weather to fires, through a robust weather–fire relationship<sup>14</sup>. This challenge hinders a

<sup>1</sup>Department of Compound Environmental Risks, Helmholtz Centre for Environmental Research—UFZ, Leipzig, Germany. <sup>2</sup>College of Water Sciences, Beijing Normal University, Beijing, China. <sup>3</sup>Department of Hydro Sciences, TUD Dresden University of Technology, Dresden, Germany. ✉e-mail: [fengsf@mail.bnu.edu.cn](mailto:fengsf@mail.bnu.edu.cn); [emanuele.bevacqua@ufz.de](mailto:emanuele.bevacqua@ufz.de)

comprehensive assessment of observed extreme fire dynamics resulting from climate change.

Recognising this challenge, recent studies have extended their focus from fire weather attribution to fire attribution by employing various statistical<sup>16,17</sup> or process-based models<sup>18</sup> to link weather with fire activity. These studies revealed an increase of observed burned areas during fire events due to human-induced climate change over areas such as Canada<sup>19</sup>, western United States<sup>17</sup>, California<sup>16,20,21</sup>, and equatorial Asia<sup>22</sup>. Despite the progress, many of these regional studies mainly focussed on the effect of increasing temperature on fires, without considering possible changes in other meteorological drivers of fires<sup>16,20</sup> such as precipitation, relative humidity, and wind (see Table S1). A recent study attributed global simulated burned area changes to climate change in multiple relevant fire weather drivers based on process-based fire models of the Inter-Sectoral Impact Model Intercomparison Project (ISIMIP)<sup>18</sup>. However, the identified change in the study can be partially due to internal climate variability and, therefore, cannot be solely attributed to human-induced climate change<sup>23</sup>. Furthermore, it is unclear how individual changes in different fire meteorological drivers contributed to extreme fire changes. Overall, despite these important recent advances, large-scale systematic efforts to attribute observed extreme fires to human-induced climate change remain limited.

Here, by combining observed burned area from the GFED4 Database<sup>24</sup> with FWI derived from ERA5 reanalyses<sup>25</sup> and output from climate models<sup>26</sup>, we quantify the effect of human-induced climate change on the likelihood of more than 700 regional weekly fire extreme occurrences (see Fig. S1 for a schematic of the approach). For each extreme fire, we quantify—given the observed meteorological conditions during the fire—how human-induced climate change affected the probability of the extreme fire occurrences. In practice, by focusing on the fire season during 2002–2015, we identify a relationship between observed weekly fire extremes and FWI by using a logistic regression that, for each week, enables predicting the probability of regional extreme fire occurrences based on FWI. Focusing on regions with good predictability, we then use the considered relationship to quantify the human-induced climate change effect and its change over time by comparing the predicted probability of extreme fires under observed factual climate conditions and counterfactual conditions without human-induced climate change. Finally, we partition the human-induced climate change effect on extreme fires into contributions arising from changes in different meteorological drivers of FWI.

## Results

### The FWI can predict regional weekly fire extremes

To attribute observed extreme fire to human-induced climate change, we first identify a weather-fire relationship at the weekly scale over the Intergovernmental Panel on Climate Change (IPCC) regions. That is, for each IPCC region, and by focusing on the fire season, we use a logistic regression model to predict the probability of regional weekly extreme fire as a function of regional weekly FWI (hereinafter regional model; see ‘Methods’). Fire extremes are defined based on the 85th percentile of the regionally aggregated weekly burned area—note that while we refer to *regional fires*, these events are likely to encompass multiple small-scale events within a given region. The focus on weekly fires was taken because large fires generally extend beyond a single day<sup>8</sup>, whereas considering monthly or seasonal fires within the fire season would yield a limited sample size. For the spatial scale, considering the regional scale helps with reducing the effect of internal climate variability when quantifying the human-induced climate change influence on climatic fire drivers<sup>27</sup>. Finally, we note that although aggregating FWI at the regional scale could cancel out local fire weather conditions behind small-scale fires and potentially ignore FWI-BA relationships on a smaller scale, such a regional scale still provides better model performance when we compared it with a logistic regression calibrated at the weekly and grid-scale (see Supplementary information, section 1).

The skill of the regional model is not uniformly high across all IPCC regions (Fig. 1a). Therefore, in the following, we select 19 out of 43 IPCC regions with reliable predictions (Fig. S2a), defined as those where the

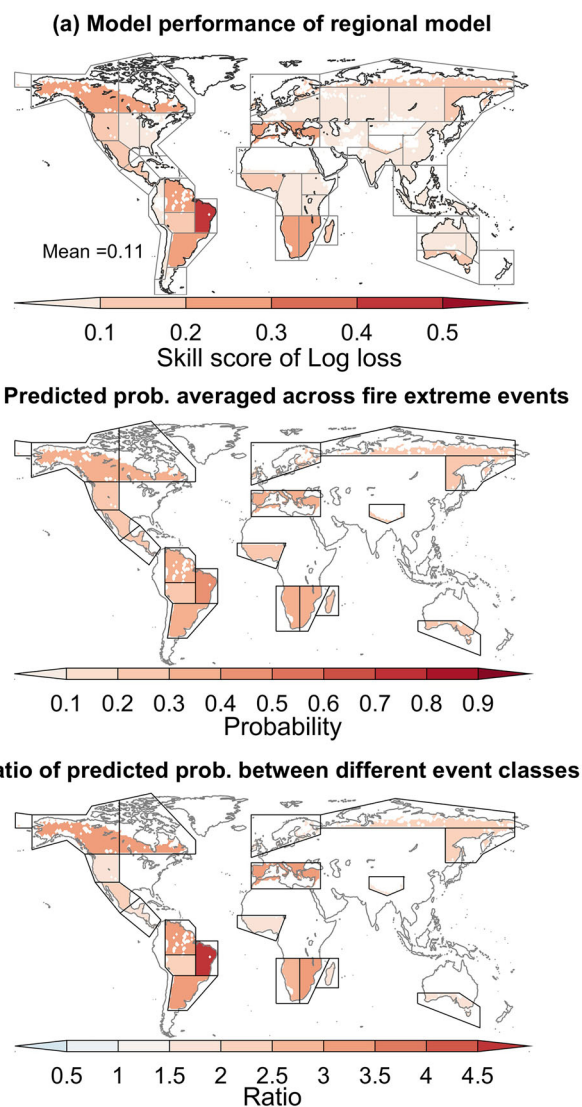


**Fig. 1 | Performance of the regional logistic regression models at predicting the probability of weekly fire extremes based on observed Fire Weather Index (FWI) during fire seasons of 2002–2015.** **a** The skill score of Log-Loss from the regional model (the number on the bottom-left indicates the average across regions); the score is shown for each IPCC region over grid cells with at least one day of positive burned area during 2001–2015. Extreme fire events are defined based on the 85th percentile of the regional weekly burned areas time series during fire season. **b** The predicted probabilities of extreme fire averaged across all observed extreme fire events, based on the regional logistic model. **c** The ratio of predicted probabilities averaged across observed extreme fire events to that averaged across non-extreme fire events (including weeks with zero regional burned area); a ratio above one indicates the model's ability to discern between these two event classes. Polygons in panel (a) show all IPCC regions initially considered for the regional model, and those in panels (b, c) indicate only those selected for the follow-up attribution analysis due to the relatively good model's skill.

Log-Loss skill score exceeds the 0.1 value<sup>16</sup> (a value above zero indicates better performance than a model predicting the baseline probability of extreme fire). Note that these selected regions also show good performance with other skill scores such as Brier Score (BS) and Precision-Recall Area Under the Curve (PR-AUC) (Fig. S2b). For the selected regions, to further intuitively inspect whether the model can distinguish between conditions that favour extreme fires, we compared the predicted probability of regional extreme fire occurrence averaged across actually observed extreme fire events and averaged across non-extreme events. The predicted probabilities averaged on actual extreme fires (Fig. 1b) is

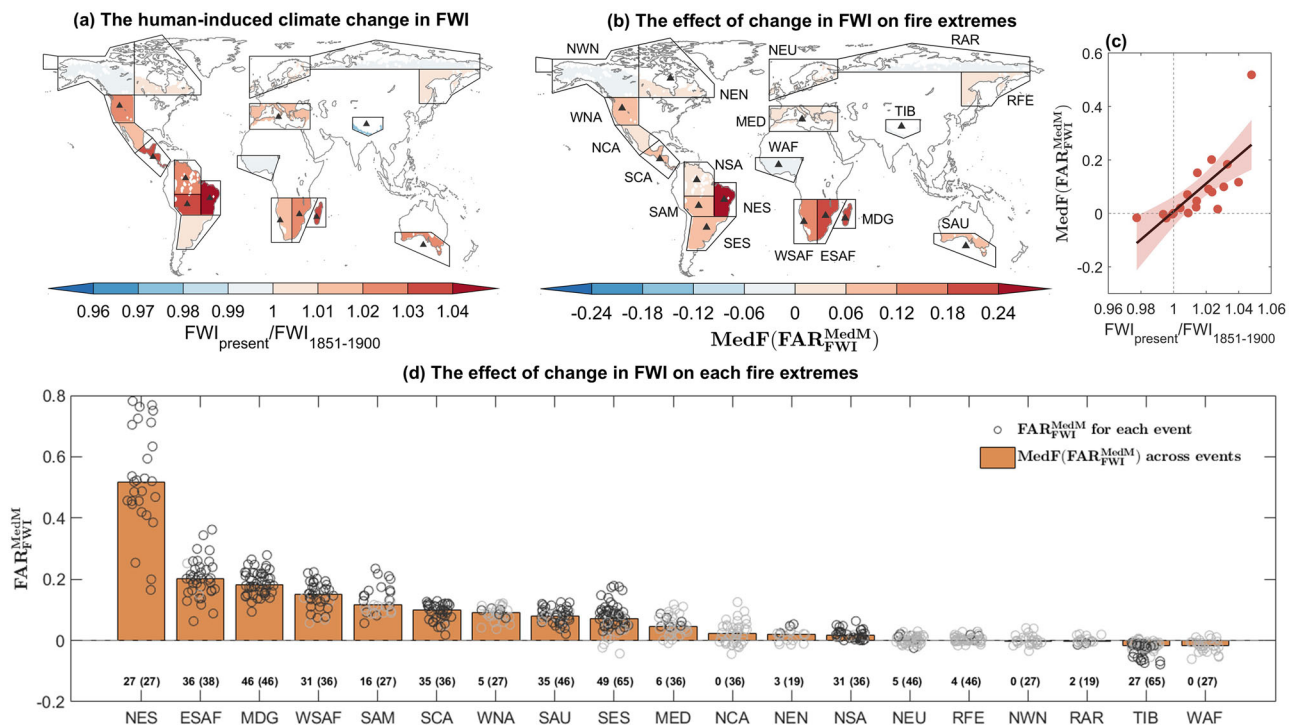


**Fig. 2 | The contribution of human-induced climate change on regional extreme fires over selected regions. a** The multimodel median change in FWI during the fire season, defined as the ratio of conditions in 2002–2015 to preindustrial conditions in 1851–1900 over selected IPCC regions (regional values are derived based on the median of the ratio across grid cells of each region; see ‘Methods’). **b** The human-induced climate change influence on the predicted probability of observed extreme (>85th percentile) fire events during fire seasons of 2002–2015, defined as the fraction of attributable risk (FAR), which is obtained by first computing the median of the FAR across climate models for individual extreme fires and then the median across fire events ( $MedF(FAR_{FWI}^{MedM})$ , see ‘Methods’). FAR values above 0 indicate that human-induced climate change made extreme fire events more likely. The black triangle in panel (a) indicates that over 75% of climate model outputs agree on the

direction of change (ratio above or below 1), while in panel (b) it indicates the same level of agreement on the sign of the change among extreme fire events. **c** The scatter plot of multimodel median of change in FWI from panel a (x-axis) and  $MedF(FAR_{FWI}^{MedM})$  from panel b (y-axis), including the linear regression line with shading for its two-sided 95% confidence interval. **d** Over selected regions (x-axis), individual grey points show the multimodel median of human-induced climate change influence on individual extreme fire events ( $FAR_{FWI}^{MedM}$ , y-axis), with orange bars showing the median across events ( $MedF(FAR_{FWI}^{MedM})$ , the same shown in panel b). Black points mark fire events for which more than 75% of climate models agree on the sign of  $FAR_{FWI}^{MedM}$ . The numbers on the bottom indicate the number of black points, followed by the total number of analysed events in brackets.

0.31, that is 31%, on average across selected regions. Although 31% may not appear very high, in line with the not-very-high skill score of the regional logistic regression model, it reflects the fact that large fire occurrence is a complex process, which, in addition to fire weather represented here, depends on fuel load, which is only partially accounted for via FWI, ignition sources availability, and fire response efforts. Nevertheless, the predicted probability of 31% actually implies a relevant risk of fire extremes under specific fire weather, as shown by the fact that such a probability is about 2.6 times higher than during non-extreme fire events on average (Fig. 1c). Overall, these prediction skills over the 19 selected regions indicate that the logistic regression model provides a good relationship linking fire weather and extreme fire occurrence for carrying out a climate change attribution analysis.

### Human-induced climate change effects on regional extreme fires

Grounded in the considered weather–fire relationship, we investigate the effect of human-induced climate change on extreme fires. To this end, we first inspect the human-induced climate change in FWI derived from climate models output of the Coupled Model Intercomparison Project Phase 6 (CMIP6) (Fig. 2a). FWI increases widely worldwide, with 15 out of the 19 IPCC regions showing an increase during the fire season according to the multimodel median. In particular, 10 regions show a robust increase, that is, with 75% of models agreeing on the positive change. The increase is particularly pronounced in North-Eastern South America (NES), South Central America (SCA), and South American Monsoon (SAM). While such increases in FWI during the fire season suggest that climate change may

have increased the fire potential<sup>10</sup>, it remains unclear to what extent this FWI increase contributes to fire extremes.

To quantify the role of the human-induced climate changes in FWI on observed extreme fire events, we remove the above human-induced climate change from observed FWI and exploit the weather–fire relationship derived from the logistic regression model. Specifically, we computed the fraction of attributable risk (FAR) based on predicted probabilities of extreme fires from the logistic regression model. For each extreme fire event  $n$ , we computed the  $FAR_{FWI}^n$  as  $\frac{p_{FWI}^n - p_{FWI0}^n}{p_{FWI}^n}$ , where  $p_{FWI}^n$  and  $p_{FWI0}^n$  are the probabilities of each extreme fire based on observed factual FWI derived from ERA5 reanalysis and counterfactual FWI obtained by removing climate-models-based trends from reanalysis, respectively (see ‘Methods’ and Table S2 for detailed definitions on the symbols used). In total, across regions, our setting enables the computation of the FAR for 705 extreme fire events, with a range of 19–65 events across individual regions (Fig. 2d; note that these numbers depend on the 85th percentile threshold used to define extremes and the length of regional fire season). To synthesise information from multiple fire extremes and climate models, for each region we computed  $MedF(FAR_{FWI}^{MedM})$ —we first computed multimodel median of  $FAR_{FWI}^n$  for each extreme fire event ( $FAR_{FWI}^{MedM,n}$ , which hereinafter is referred to as  $FAR_{FWI}^{MedM}$  for simplicity) and then computed the median of such multimodel medians across fire events. At the global scale, averaged across the selected IPCC regions, the  $MedF(FAR_{FWI}^{MedM})$  is approximately 0.08. Note that this value is about identical if we alternatively invert the order of the median operations across fires and climate models—this alternative approach allows for quantifying the uncertainty arising from differences



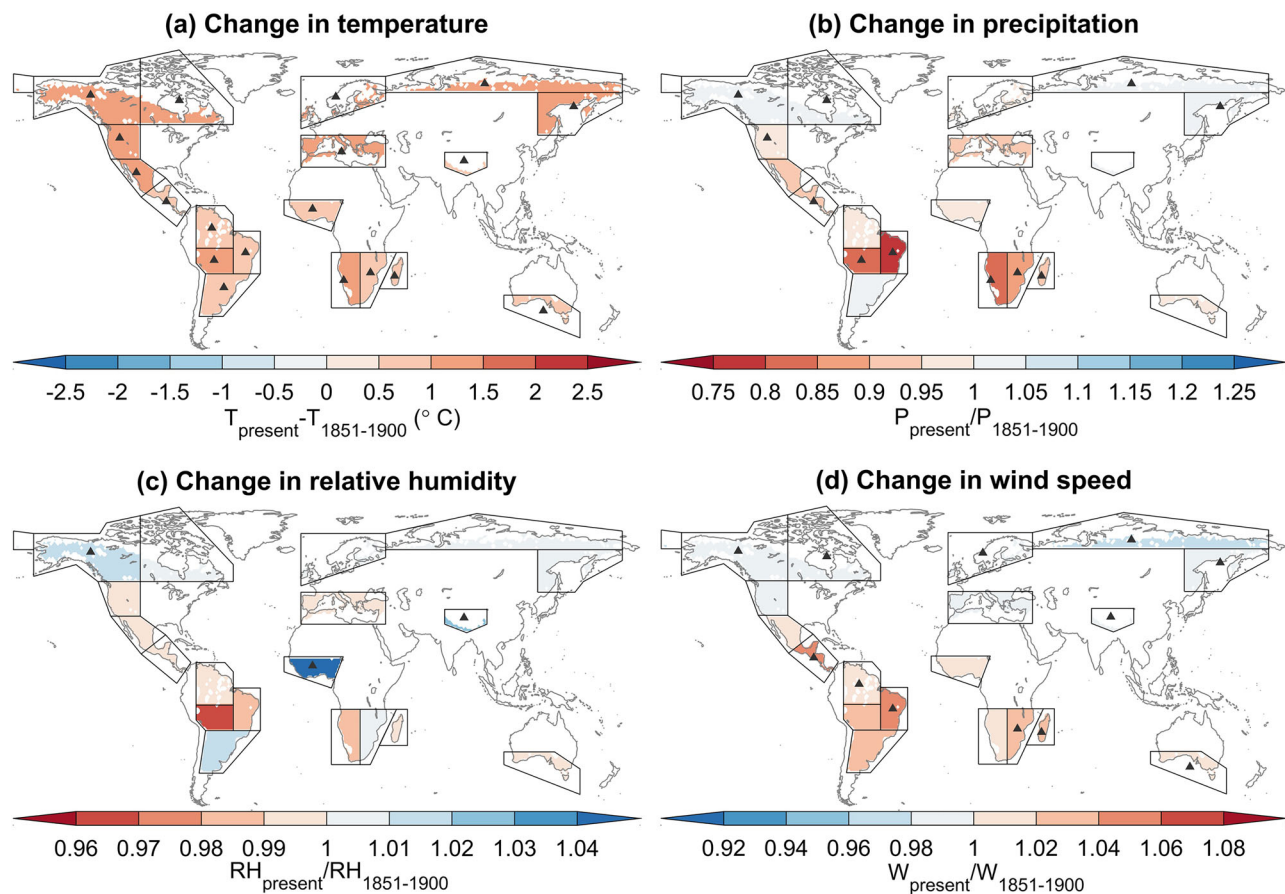


**Fig. 3 | Human-induced climate change in temperature (T), precipitation (P), relative humidity (RH), and wind speed (W) over selected IPCC regions. a** The multimodel median change in maximum temperature during the fire season, defined as the difference between conditions in 2002–2015 and preindustrial conditions in 1851–1900 (see ‘Methods’). The regional values are derived from the median of the

difference across grid cells of each region (see ‘Methods’). **b–d** The same as panel a, but for multimodel median change in precipitation (**b**), minimum relative humidity (**c**), and wind speed (**d**), defined as the ratio of conditions in 2002–2015 to preindustrial conditions in 1851–1900. The black triangles indicate that more than 75% of climate models agree on the direction of the change.

among the 14 climate models, yielding a standard deviation (SD) of 0.04 (see ‘Methods’). Overall, we thus conclude that human-induced climate change was responsible for  $8 \pm 4\%$  of the probability of regional extreme fires on average. This contribution varies across IPCC regions (Fig. 2b) and aligns in sign with the change in FWI (Fig. 2c), with positive contributions over 15 out of 19 regions.

The largest increase in extreme fire probability from human-induced climate change is found in North-Eastern South America (NES) with a FAR of 0.52 [0.17–0.78, range across extreme fire events], followed by East Southern Africa (ESAF, 0.20 [0.06–0.36]), Madagascar (MDG, 0.18 [0.09–0.28]) (Fig. 2d). Over these three regions, for almost all individual fire extreme events, 75% climate models agree that the FAR is positive (see black points in Fig. 2d). In contrast, human-induced climate change slightly decreased the median probability of extreme fires across observed events over North-Western North America (NWN), Western Africa (WAF), Russian Arctic (RAR), and Tibetan Plateau (TIB). Finally, we note that the FAR is independent of model performance and fire season length given a fixed change in FWI (Fig. S3), providing confidence in the interpretation of the spatial variations of FARs across IPCC regions.

### Human-induced warming is the main driver of the increasing fire risk

Previous fire-attribution studies typically quantified the effect of human-induced climate change on fire by considering the effect of human-induced changes in single meteorological drivers (see Table S1), for example, changes in temperature<sup>16,20</sup> or precipitation<sup>22</sup>. However, human-induced climate change can alter several variables affecting fire weather dynamics at once, as

shown by changes in the meteorological drivers of FWI, that is, temperature, precipitation, relative humidity, and wind speed (Fig. 3). Consistent with unequivocal human-induced warming, temperature increased significantly during fire season over IPCC regions (Fig. 3a), which can result in drier soils via enhanced evaporation<sup>28</sup>, thereby diminishing moisture in combustible materials and heightening their vulnerability to ignition. In contrast, changes in precipitation, relative humidity, and wind vary widely across IPCC regions. In particular, changes in precipitation and relative humidity have similar signs in changes with decreases that can contribute to the fire severity and extent<sup>29,30</sup> in most regions, for instance, North-Eastern South America (NES), South American Monsoon (SAM), West Southern Africa (WSAF), and Southern Australia (SAU) (Fig. 3b–c). Wind speed, which can alter the pace of fire spread<sup>31</sup>, decreases over high-latitude regions and increases elsewhere (Fig. 3d). These spatial differences in the changes of fire weather drivers indicate that the contribution of weather changes on fire extremes can be heterogeneous across regions.

To quantify the effect of individual changes in the four meteorological drivers on the probability of extreme fire changes, we recompute FARs based on counterfactual FWI obtained after removing human-induced climate change signals in one driver at a time<sup>28,32,33</sup> (that is, *one-factor-at-a-time method*). To inspect whether this approach can provide insights into the relative contributions of the four drivers, we compare the sum of the separate FARs based on changes in the individual drivers ( $MedF(\text{Sum}(\text{FAR}_{\text{driver}})^{MedM})$ ) in Fig. S4a with the FAR based on actual changes in the FWI itself ( $MedF(\text{FAR}_{FWI}^{MedM})$ ) in Fig. 2b (see ‘Methods’ and Table S2 for detailed definitions on the symbols used). While the former FAR tends to overestimate the latter FAR (Fig. S4c), the high inter-regional

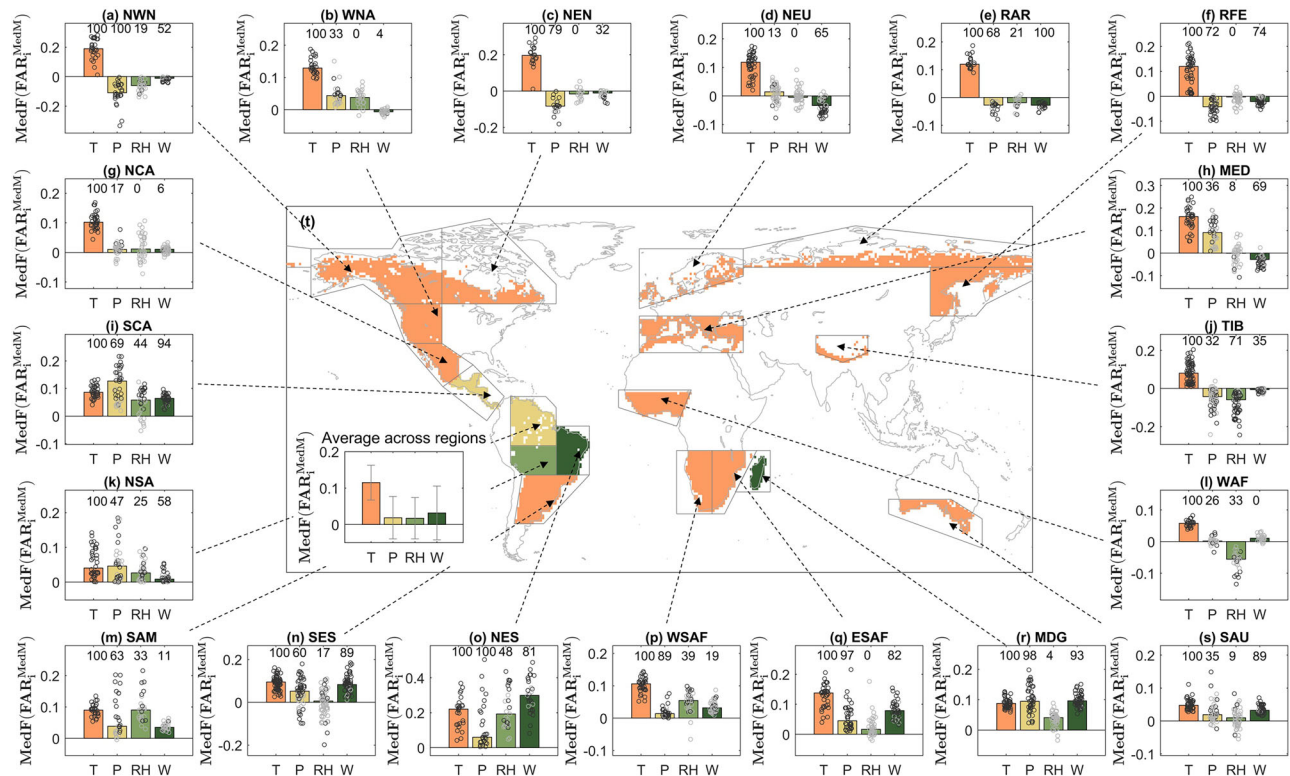


**Fig. 4 | The contributions of human-induced climate change in individual FWI meteorological drivers to regional extreme fires. a–s** For selected IPCC regions, the fraction of attributable risk (FAR) for observed extreme fires during the fire seasons of 2002–2015, based on four counterfactual FWIs where the changes in temperature ( $i = T$ ), precipitation ( $i = P$ ), relative humidity ( $i = RH$ ), and wind speed ( $i = W$ ) were removed once at a time. Bars show  $MedF(FAR_i^{MedM})$ , which is obtained by first computing the median of the FAR across climate models for individual extreme fires and then the median across fire events (see ‘Methods’). Points indicate the FAR

values for individual fire events ( $FAR_i^{MedM}$ ), with black indicating events where more than 75% of climate models agree on the FAR sign (the fraction of black points to the total number of points is indicated by the numbers on top). **t** Over different regions, the driver whose changes have the largest effect on fire occurrence, that is the driver with the largest absolute value of the FAR. The barplot on the bottom-left shows the  $MedF(FAR_i^{MedM})$  averaged across selected regions for each driver, and the error bars indicate the one standard deviation range of  $MedF(FAR_i^{MedM})$  across regions.

correlation between the two FARs ( $R = 0.93$ ) supports our approach. Note that such an overestimation, rather than merely arising from a potential non-linear response of the predicted fire extremes’ probability (and therefore of the FAR) to changes in FWI, may be largely due to some interaction between changes in individual drivers. This is suggested by the fact that the FAR based on counterfactual FWI obtained by removing human-induced change from all FWI meteorological drivers at once ( $MedF(FAR_{all\ drivers}^{MedM})$ , see ‘Methods’) also overestimates the FAR based on the actual changes in the FWI itself ( $MedF(FAR_{FWI}^{MedM})$ ) (Fig. S4b, d). This finding highlights that accounting for human-induced climate change in individual fire drivers separately, as often done in previous studies (see Table S1), may lead to overestimating the human-induced climate change effect due to the missing consideration of compensating effects from the interaction between changes in fire drivers.

By implementing our approach, we find that human-induced warming plays the most important role in shaping changes in fire extremes, leading to a FAR of 0.12 on average across regions (Fig. 4t, bottom-left). That is, our approach indicates that human-induced warming was responsible for about 12% of the probability of regional extreme fires on average during the fire season of 2002–2015. However, at the regional scale, changes in relative humidity, precipitation, and wind additionally modulate the homogeneous increase in fire risk caused by warming (Fig. 4a–s). This additional modulation can compensate warming effects or even result in a slight climate change-induced reduction of fire risk over some regions (Fig. 2b). For instance, the compounding effects of higher precipitation and relative humidity with weaker winds over North-Western North America (NWN), Russian Arctic (RAR), and Tibetan Plateau (TIB) (Fig. 3b, c, d) slightly reduced the probability of extreme fires, despite the increasing fire risk from

higher temperature (Fig. 4a, e, j). In addition, over Western Africa (WAF), a decrease in fire probability induced by higher relative humidity compensates for the increase from warming (Fig. 4l), overall resulting in a slight reduction of the fire risk (Fig. 2b). Overall, these findings underscore that fire risk increases due to human-induced warming, but changes in other meteorological drivers substantially modulate the temperature-driven increase, even slightly reversing it in some regions.

### Rising human-induced climate change impact on extreme fires

Due to ongoing emissions, climate change effects, including warming, are increasing over time<sup>34</sup>, raising the question of whether climate change impacts on fire extremes have become more and more evident over time. To address this question, for each region, we quantified temporal trends in the FAR across individual extreme fire events ( $FAR_{FWI}^{MedM}$ ). Our findings reveal an upward trend in FAR across 14 out of 19 IPCC regions (Fig. 5a). Among these, 6 regions show a significant increase ( $p$ -value  $< 0.05$  from Fig. S5), alongside a positive median human-induced climate change effect across all extreme fires ( $MedF(FAR_{FWI}^{MedM}) > 0$ , Fig. 2b). In contrast, no region shows a significant decreasing trend in FAR. Russian Arctic (RAR) and Tibetan Plateau (TIB) show a negative but not significant trend in FAR across events (Fig. S5), which, together with a median reduction of fire risk across events ( $MedF(FAR_{FWI}^{MedM}) < 0$ , Fig. 2b), indicates an ongoing reduction of fire risk. Over Northern Central America (NCA), West Southern Africa (WSAF), and South Asia (SAU), while the declining trend in FARs coupled with the positive  $MedF(FAR_{FWI}^{MedM})$  may suggest that the increased fire risk from human-induced climate change has peaked and is now decreasing, we underscore that FAR trends are not statistically significant and less than 75% of models agree on the decreasing trends.

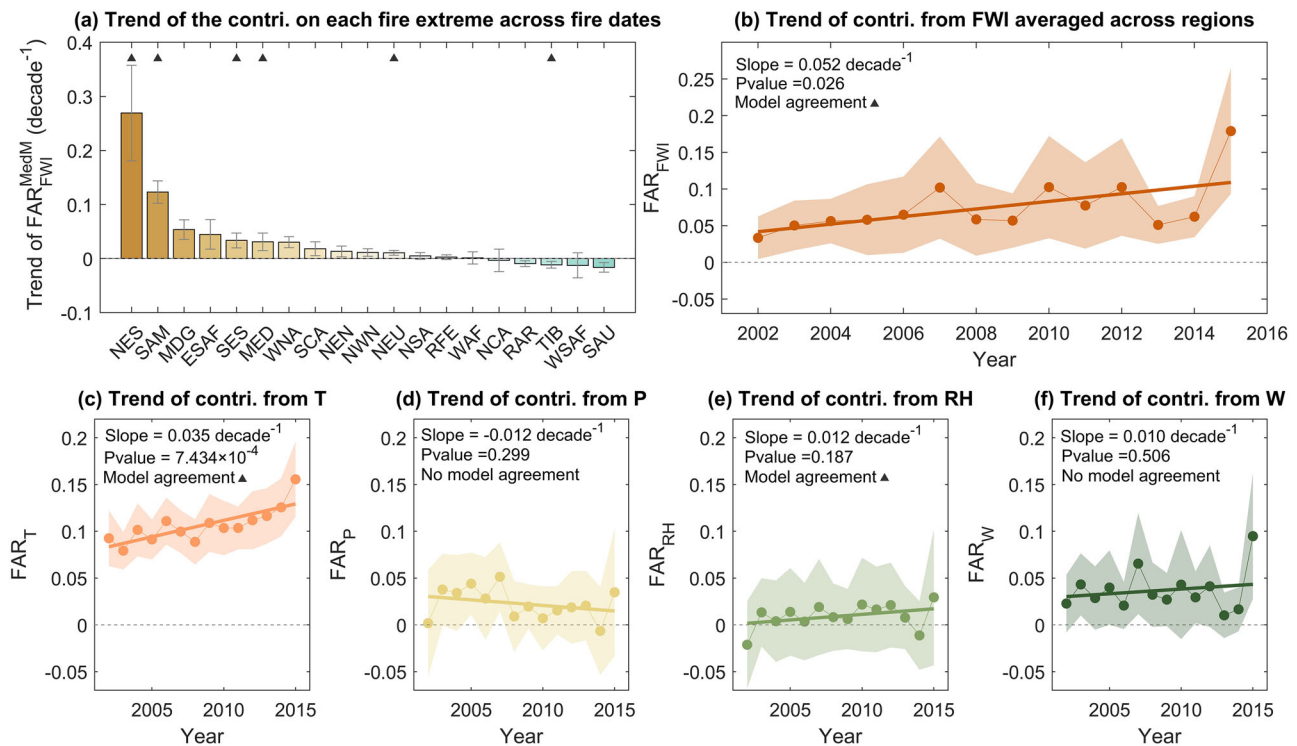


**Fig. 5 | The trend of the contribution of human-induced climate change on the probability of regional extreme fires during the fire season of 2002–2015. a** For individual regions (x-axis), the y-axis shows the linear trend value of  $FAR_{FWI}^{MedM}$  over fire dates, where  $FAR_{FWI}^{MedM}$  is the multimodel median of the effect of human-induced climate change in FWI on the predicted probability of an individual extreme fire event (grey bar shows the  $\pm 1$  standard error of the regression line; see ‘Methods’). The black triangles indicate regions where over 75% of climate models agree on the sign of trend. **b** The annual impact of human-induced climate change in FWI on the probability of extreme fire events, obtained by first averaging  $FAR_{FWI}$  across all fires

of all regions for each year given one climate model and then getting multimodel median—the shading indicates  $\pm 1$  standard deviation of annual global FAR from multiple climate models. The trend is illustrated by the linear regression line, with the numbers in the panel showing the slope of the regression line and its p-value. The black triangle indicates that over 75% of climate models agree on the sign of trend. **c–f** Similar to panel b but for the annual contribution of human-induced climate change on the probability of extreme fire events based on four FWI counterfactuals where the trend of temperature (**c**,  $FAR_T$ ), precipitation (**d**,  $FAR_P$ ), relative humidity (**e**,  $FAR_{RH}$ ), and wind speed (**f**,  $FAR_W$ ) was removed once at a time (see ‘Methods’).

Despite the regional variations in the sign of the FAR trends, which is consistent with heterogeneous trends in fire weather, at the global scale, a significant positive trend of 5.2% per decade emerges ( $p$ -value = 0.026; Fig. 5b). Such a FAR trend combined with the 8% contribution on fire extreme we presented earlier (Fig. 2b) indicates the human-induced climate change effect has been accelerating. This is because a linear increase in FAR of 5.2%/decade since the preindustrial period would yield an average contribution well above 8% during 2002–2015. Thus, FAR likely increased slowly initially and accelerated in the last decades, consistent with the changes in FWI since the preindustrial period (Fig. S6). We find that this FAR trend at the global scale is dominated by increasing temperature, contributing to a significant increase of 3.5% per decade in the FAR (Fig. 5c). In contrast, at this global scale, the contributions of the other three drivers show no significant trend (Fig. 5d–f), in line with spatially heterogeneous effects of these three drivers (Fig. 4). Finally, we note that the confidence in the decomposition of the trends is supported by the consistent temporal dynamics of the trends found when inspecting the sum of the separate FARs based on changes in the individual drivers ( $Sum(FAR_{driver_i})$ ) and the FAR based on changes in all drivers at once ( $FAR_{all\ drivers}$ ), which exhibit trends of 7.0% and 4.8% per decade, respectively (Fig. S4e, f).

## Discussion

Combining observations and climate model outputs, our study revealed that in the fire season of 2002–2015, human-induced climate change contributed 8% of the predicted probability of more than 700 regional observed extreme fires on average across regions, with a large contribution in some regions including North-Eastern South America (52%) and East Southern Africa (20%). This study advances our understanding of the role of human-

induced climate change in extreme fire occurrences at the global scale by focusing on actual burned areas rather than on the typically considered fire-conducive weather extremes<sup>10,35</sup>. Building on previous works<sup>16,20,21,36</sup>, to move from attributing fire weather extremes to actual extreme burned areas, we expanded the conventional FAR framework through a logistic regression that links fire weather to extreme fire (Fig. S1). We note that although we selected regions with good predictive skills for the attribution analysis, skills are not very high in line with the complex nature of fire dynamics, which is modulated not only by climatic drivers but also by fuel load—partially captured by FWI—and direct human activities, such as ignition sources and response actions. Accordingly, our attribution focuses exclusively on the human-induced climate change driver of extreme fires. In this context, we also note that although FWI is a widely used weather indicator for fire danger<sup>37</sup>, our FWI-based approach may neglect climate change effects on fires mediated by weather factors not captured by FWI, like solar radiation.

To create counterfactual weather conditions, we applied changes in mean monthly-scale climatic variables (that is, scaling factors) from climate models<sup>28,32</sup> to daily observed variables, in line with the so-called delta approach<sup>38,39</sup>. While changes in mean conditions may not necessarily reflect extreme events’ dynamics, our approach aligns with previous studies<sup>32</sup> and some analyses showing similar changes in mean temperature and extreme temperature at daily scales for some events<sup>40</sup>. Furthermore, long timescales are also relevant for the build-up of extreme fire weather conditions<sup>41</sup>. Tailoring the approach to changes in individual meteorological drivers allowed us to investigate the effect of human-induced climate change in precipitation, temperature, relative humidity, and wind speed on extreme fires. While we found that human-induced climate change warming dominates the increased fire risk on average globally (Fig. 4), inspecting



many individual regions separately enabled revealing areas with large contributions from human-induced climate change in other drivers. For instance, over North-Eastern South America (NES), our results show that changes in the extreme fire are primarily driven by changes in wind speed, a driver of changes that has received limited attention so far; while hotter and drier conditions have increased fire risk over Southern Central America (SCA), Northern South America (NSA), South American Monsoon (SAM), and West Southern Africa (WSAF) (Fig. 4). Identifying such contributions from specific drivers advances our understanding of climate change effects on fire, given that such contributions were overlooked by many of the existing attribution studies (see Table S1). In addition to the importance of considering change in all fire drivers, exploiting the fact that our study involved the analysis of FWI, we could assess the relevance of considering the interaction between changes in the drivers. We found that human-induced climate change effects from the simulated change in all FWI drivers (without interactions) exceed those derived from actual simulated changes in FWI itself (with interactions) (Fig. S4a–d). This highlights that current fire attributions based on detrending methods that cannot account for such interaction may provide misleading insights into the human-induced climate change effect. Taking a broader perspective, although accounting for these interactions might be challenging in practice, these insights can be valuable for other fire-attribution studies and projects that routinely detrend individual variables separately, for instance, the ISIMIP project<sup>18</sup>.

Given the importance of climate models to quantify human-induced climate change, our approach exploits multiple climate models. As typical for attribution studies based on models, the results depend on the ability of the climate model ensemble to represent human-induced climate change trends in the FWI and its drivers, whereas over certain regions, discrepancies between historical trends in observations and models have been observed, which may be due to model biases and/or internal climate variability<sup>42–44</sup>. Here, separately employing multiple climate models provides insights into uncertainties around the contribution of the FWI and individual drivers due to climate model structure and natural climate variability (Fig. S7).

Our findings distilled an increasing climate change effect on burned area extremes at the global scale, which is strengthened by a recent attribution of monthly-scale fires based on process-based fire models within the framework of the ISIMIP project<sup>18,23</sup>. Although a direct comparison of the numbers derived in the two studies is challenging because of the different spatial-temporal scales considered, a difference lies in the detrending methods. The recent study<sup>18</sup> separately detrended multiple observed weather variables to generate counterfactual climates, which cannot isolate human-induced climate change<sup>23</sup> as observed trends also encompass internal climate variability, particularly at the regional scale<sup>45</sup>. For instance, such a detrending approach<sup>23</sup> indicates cooling in Madagascar despite ongoing human-induced warming (Fig. 3a). In our study, we did not consider socioeconomic factors that were considered by other studies<sup>18,46</sup>, which are relevant drivers of fire changes in some regions. For instance, while we found an increasing fire risk under human-induced climate change, regions such as North-Eastern South America and the Caribbean have witnessed a decrease or no change in burned area<sup>18,47</sup>, possibly due to socioeconomic factors like agricultural expansion and intensification<sup>7,18</sup>. This finding underscores the importance of socioeconomic development in fire management and suggests that the incidence of extreme fires could be even more pronounced in the absence of such interventions<sup>18</sup>.

Together with an average global human-induced climate change contribution of 8% on the probability of extreme fires during 2002–2015, we also found that such a contribution increased by 5.2%/decade over the same period, primarily driven by rising temperature (3.5%/decade; Fig. 5). Put together, the 8% contribution and the 5.2%/decade trend, indicate that the human-induced climate change effect has emerged substantially only recently and is now growing over time, in line with accelerating warming (Fig. S6) resulting from emissions of greenhouse gases<sup>18</sup>. Thus, while burned areas have declined over the last decades in several regions due to agricultural expansion and intensification<sup>7</sup>, our results indicate that

compensating for the growing climate change effect may become more challenging over time. Such emergent climatic effects pose significant challenges for ecosystems and human populations over most regions worldwide, where plants, animals, and human beings suffer from extreme fire. Coping with quickly emerging climate change effects requires important adaptation efforts. Solutions are in our hands, calling for urgent climate mitigation and adaptation strategies, including effective fire management and actions to build resilience in vulnerable areas.

## Methods

### Observed burned area and climate reanalyses

We obtained daily burned areas (BA) with 0.25° spatial resolution for 2001–2015 from the Global Fire Emissions Database version 4 (GFED4)<sup>24</sup>—note that the daily BA dataset from GFED5 is not yet available. We re-gridded this data to the one-degree resolution to ensure consistency with the following climate model simulations.

We collected daily meteorological data from the ERA5 reanalysis dataset<sup>25</sup>, that is, temperature, relative humidity, wind speed at noon local time, and total precipitation, which serve for computing the Fire Weather Index (FWI) (0.25° spatial resolution). Here, relative humidity was obtained from temperature and dew point temperature following the equation from ref. 48. Note that building on previous work<sup>49</sup>, we truncated the relative humidity to 100% in a few rare cases where it slightly exceeded this value before computing the FWI. The 10m wind speed was derived from the 10m u and v wind components. We also aggregated the above four meteorological variables into a one-degree resolution to match the following climate model simulations. Then, we employed the meteorological data to compute the FWI following the guidelines provided by the European Centre for Medium-Range Weather Forecasts (ECMWF)<sup>49</sup>; this was implemented with the support of some of the code from ref. 50.

### Climate model simulations

To compute FWI from climate models, we collected daily precipitation (*pr*), maximum daily temperature (*tasmax*), mean daily wind speed (*sfcWind*), and minimum daily relative humidity (*hursmin*). Note that maximum temperature and minimum relative humidity are alternatives to noon variables employed for ERA5<sup>50</sup>, which ensures that more climate models from Coupled Model Intercomparison Project Phase 6 (CMIP6) can be used (see Table S3 for a list). This resulted in 14 models that provide all the necessary variables for the historical period (1851–2014) and the Shared Socioeconomic Pathways SSP3-7.0 scenarios (which were concatenated to the historical simulations from 2015 onward). We selected the SSP3-7.0 scenario as it closely matches emissions over the past decade<sup>51</sup>. These simulations were re-gridded to a common one-degree resolution before the computation of FWI. Additionally, we employed fifty ensemble members from the CanESM5 model to assess the contribution of internal climate variability on the uncertainties in the effect of human-induced climate change in FWI and the associated meteorological drivers on fire extremes (Fig. S7).

### Definition of fire season

To define the fire season at the regional scale, we first focused on the grid cells that experienced BA for at least one day from 2001 to 2015 (other grid points are set into NaN and not considered in the study) and then aggregated gridded BA into 43 IPCC reference regions<sup>52</sup>. In each region, we first computed the monthly distribution of BA from daily data across multiple years (2001–2015) and then defined the fire season as the fewest consecutive months that account for at least 80% of the total BA during the period 2001–2015 (Fig. S8). As a result, for some regions, the fire season spans across two calendar years, which results in one fire season less than the length of available calendar years, that is the 15 years during 2001–2015 (this is because incomplete fire seasons at the edge of the time series, in 2001 and 2015, were not considered). To ensure that all analysed regions have the same number of fire seasons, we excluded the fire season in 2001 for regions where the fire season spans across the same calendar year. Then, we labelled

a fire season with the year of its last month and used the fire season labelled 2002 to 2015 for further analyses.

### Logistic regression of extreme fires onto FWI

To establish a robust weather–fire relationship<sup>16,53,54</sup>, we chose to analyse fire at the IPCC regional and weekly scales after some considerations and analyses described below.

For the spatial scale, we chose the regional scale after assessing that the weather–fire relationship during fire season generally works better when considering BA and FWI aggregated over IPCC regions than at individual grid cells (see supplementary information). Such regional scale also enables reducing the effect of internal climate variability on estimated human-induced climate change in climatic fire drivers<sup>27</sup>. Note that while we refer to *regional fires*, such events based on aggregated BA in a given IPCC region can be composed of multiple small-scale events within the region. At the regional scale, we employed regionally aggregated BA over IPCC regions and computed spatial median FWI over selected grid cells (where the BA was above zero for at least one day during 2001–2015) within each IPCC region (the median is preferred to the mean as it is less influenced by outliers).

For the temporal scale, the weekly scale was chosen based on the following considerations. A shorter scale than weekly, such as daily, would not be an optimal choice because the uncertainty in the burned date of the daily BA during the fire season is generally larger than one day (Fig. S9). Furthermore, large fires typically last more than a day<sup>8</sup>. In contrast, focusing on a longer time scale, such as monthly or seasonal, would limit the sample size for estimating the weather–fire relationship during the fire season, given that even the longest available monthly BA dataset within our knowledge (that is, the GFED5 product) only spans 23 years (1997–2020)<sup>47</sup>. Weekly BA and FWI were obtained by summing daily BA and averaging daily FWI over consecutive 7-day windows, respectively (if the last 7-day window of the fire season was partially outside of the season, we disregard such last window if more than four days were outside the season, otherwise we employed the missing days from the first days outside of the fire season). For each IPCC region, we first obtained spatial median daily FWI and then derived weekly FWI.

To estimate the relationship between BA and FWI, we defined extreme fire events occurrence ( $Y = 1$ ) when the time series of the weekly BA during fire season exceeds the 85th percentile of their distribution ( $Y = 0$  for non-extreme occurrence, which also includes weeks with zero BA). Although such a relatively high threshold was employed, we found that the 85th percentile of the BA is zero over New Zealand (NZ) (Fig. S10a). Therefore, we disregarded this region when modelling the FWI–BA relationship. The fraction of the total BA during fire season for 2002–2015 caused by extreme (85th percentile) fires is shown in Fig. S10b. Averaged across IPCC regions, extreme fires account for about 55% of the total BA.

Based on the selected extreme and non-extreme fire events ( $Y = 1, 0$ ), we applied a logistic regression model (hereinafter *regional model*) to estimate the probability of extreme fire as a function of FWI over selected regions:

$$\text{Logit}(P(Y = 1|FWI)) = \alpha + \beta * FWI \quad (1)$$

where  $P(Y = 1|FWI)$  indicates the predicted probability of an extreme fire event given the observed FWI;  $\alpha$  and  $\beta$  are the fitted coefficients. By computing FWI based on observed weather, including precipitation (P), temperature (T), relative humidity (RH), and wind speed (W), the regional model predicts the probability of each extreme fire event ( $n$ ) in the observed factual climate ( $p_{FWI1}^n$ ) over each region.

Model performance was evaluated using three scoring methods: the Log-Loss score (Log-Loss), the Brier Score (BS), and an area under the Precision-Recall curve (PR-AUC)<sup>16,55</sup>. For better interpretability, we

converted Raw Log-Loss and BS into skill scores, as:

$$\text{Skill score} = 1 - \frac{\text{Score}_{\text{model}}}{\text{Score}_{\text{naïvemodel}}} \quad (2)$$

A positive skill score indicates that our model outperforms a naïve model that predicts the probability of extreme and non-extreme fire using predefined values of 0.15 and 0.85, respectively (these values reflect the threshold we used to define extreme fires). As the model performance approaches perfection, the skill score approaches 1. The PR-AUC, already normalised between 0 and 1, was used in its original form. Furthermore, we tested the model's ability to discern between extreme and non-extreme fires by inspecting whether the ratio between averaged predicted probabilities across all observed extreme fire events ( $Y = 1$ ) and non-extreme events ( $Y = 0$ ) is above 1.

### The effect of human-induced climate change in FWI on extreme fires

To assess the contribution of human-induced climate change on extreme fire, we first removed climate change (identified from individual CMIP6 models) from the observed FWI time series for each grid cell following previous work<sup>28,32</sup>. Specifically, for each of the twelve calendar months and each year from 2001 to 2015, we created the counterfactual daily field of FWI by adjusting the observed field of daily FWI using a climate model-based gridded multiplicative factor. Such a multiplicative factor is defined as the ratio of monthly mean FWI in the preindustrial period (1851–1900) to the monthly mean FWI over a 15-year window centred on the considered year for each grid cell; hereinafter referred to as scaling-factor method. To visualise the human-induced climate change in FWI during the fire season over each IPCC region, we first derived the regional spatial median of the scaling factors during each month from individual models—note that such a regional median of the scaling factor is used for visualisation purposes only and not to derive counterfactual time series. Secondly, we derived the monthly median of these values across all months within fire season and finally derived the multimodel median of these values (the inverse of this quantity is shown in Fig. 2a, including information on model agreement on the direction of the change).

For each IPCC region, we derived the regional counterfactual FWI time series by computing the spatial median of the counterfactual gridded daily field of FWI. Finally, we predicted the probability of each weekly fire extreme ( $n$ ) under no climate change ( $p_{FWI0}^n$ ) by plugging the regional counterfactual FWI into the logistic regression (fitted to the factual data, following equation (1)).

Then, for each region, to quantify the contribution of human-induced climate change on extreme fire<sup>12,16</sup>, we computed the fraction of attributable risk (FAR) on each extreme fire event  $n$ , as:

$$\text{FAR}_{FWI}^n = \frac{p_{FWI1}^n - p_{FWI0}^n}{p_{FWI1}^n} \quad (3)$$

where  $p_{FWI1}^n$  and  $p_{FWI0}^n$  are the predicted probability of each extreme fire event  $n$  under observed factual and counterfactual climates, respectively (note that the total number of fire events  $N$  varies across regions because each region has different fire season lengths; Fig. S8). This FAR indicates how much of the predicted probability of extreme fire occurrence is attributable to climate change.

In a given region, we quantified the influence of human-induced climate change on a given fire extreme  $n$  as  $\text{FAR}_{FWI}^{\text{MedM}n}$  (hereinafter  $\text{FAR}_{FWI}^{\text{MedM}}$  for simplicity), which is the multimodel median of  $\text{FAR}_{FWI}^n$  based on counterfactual FWI from different climate models. The range of  $\text{FAR}_{FWI}^{\text{MedM}}$  associated with the  $N$  fire events informs on the range of climate change effects on the different fires. To summarise the results across multiple extreme fire events in a given region, we computed the median of  $\text{FAR}_{FWI}^{\text{MedM}}$  across all extreme fire events, referred to as  $\text{MedF}(\text{FAR}_{FWI}^{\text{MedM}})$ . Then we obtained the global average contribution by averaging  $\text{MedF}(\text{FAR}_{FWI}^{\text{MedM}})$



across regions. Note that we also derived such a global average FAR by alternatively inverting the order of the median operations across fires and climate models. Specifically, first, based on a counterfactual from a single climate model, we computed the median FAR across fire events for each region and then computed the global average as the average of these median values across the regions. Finally, we derived the multimodel median of the global averages and quantified the uncertainty due to model differences, represented by the standard deviation across 14 climate models.

In addition, to gain insights into the contribution of internal climate variability and climate model differences on the uncertainties in FAR over each region, we first obtained  $FAR_{FWI}^n$  for a given fire extreme over selected regions based on each member of the climate model CanESM5 in the same process we applied to each model. Then, for each fire event, we defined uncertainty due to internal climate variability as one standard deviation of FAR across 50 ensemble members from CanESM5. Similarly, differences across climate models for each fire event was quantified as one standard deviation of FAR across 14 climate models. To synthesise information from multiple fire extremes within a given region, we computed the median of such standard deviations across all events.

### The effect of human-induced climate change in FWI meteorological drivers on fires

To systematically quantify the contribution of human-induced climate change in the four individual meteorological FWI drivers (i.e., P, T, RH, and W) on extreme fires, we decomposed the human-induced climate change signal on the probability of extreme fires into that arising from changes in these individual drivers.

We first defined the human-induced climate change in individual drivers. Specifically, for P, RH, and W, we applied an analogous procedure to that explained for FWI above, that is, we employed a gridded multiplicative factor derived from pr, scfWind, and hursmin in CMIP6 models, respectively. For T, we proceeded analogously but employed a gridded additive factor from tasmax in CMIP6 models, computed as it follows. For each of the twelve calendar months and each year, the additive factor equals the difference between the monthly mean tasmax in the preindustrial period (1851–1900) and the monthly mean tasmax over a 15-year window centred on the considered year from model simulations. For individual drivers, to visualise the human-induced climate change during the fire season for each IPCC region, we first derived the regional spatial median of the scaling factors for each month from individual models. We then derived the monthly median of these values across all months within fire season; finally, we derived the multimodel median of these values (in Fig. 3, we show the inverse of such multimodel median for P, RH, W and the opposite for T).

We then obtained the counterfactual daily field of each driver by adjusting the observed gridded daily driver variables using the associated gridded monthly scaling factors defined above (derived from individual climate models). Note that, as done for factual data, we truncated counterfactual RH values to 100% in some cases where they exceeded this limit. Then, we computed four counterfactual gridded daily FWI datasets based on the four meteorological drivers—for each FWI counterfactual dataset, we applied only one counterfactual driver at a time (hereinafter *one-factor-at-a-time method*). Finally, for each IPCC region, we computed regional weekly counterfactual FWI as explained in the section above. Note that, for two models only across some dry areas during some months, scaling factors of precipitation and thus associated counterfactual values have NaN values (due to a zero denominator)—such values were disregarded when we computed regional aggregated values.

Then, based on the logistic regression fitted to observations (factual data; equation (1)), we predicted the probability of weekly fire extremes based on regional counterfactual FWI without climate change of individual drivers for each event  $n$  (hereinafter  $p_{P0}^n$ ,  $p_{T0}^n$ ,  $p_{RH0}^n$ , and  $p_{W0}^n$  for P, T, RH, and W, respectively). We then calculated the  $FAR_T^n$ ,  $FAR_P^n$ ,  $FAR_{RH}^n$ , and  $FAR_W^n$  by replacing  $p_{FWI0}^n$  in equation (3) with  $p_{P0}^n$ ,  $p_{T0}^n$ ,  $p_{RH0}^n$ , and  $p_{W0}^n$ , respectively. Finally, for each fire extreme event  $n$ , we computed the multimodel median of these FARs based on FARs from different models, that is

$FAR_T^{MedM\ n}$ ,  $FAR_P^{MedM\ n}$ ,  $FAR_{RH}^{MedM\ n}$ , and  $FAR_W^{MedM\ n}$  (hereinafter  $FAR_T^{MedM}$ ,  $FAR_P^{MedM}$ ,  $FAR_{RH}^{MedM}$ , and  $FAR_W^{MedM}$  for simplicity, respectively). To summarise human-induced climate change effects across fires, we also computed the median of such multimodel median values across all fire extreme events, referred to as  $MedF(FAR_T^{MedM})$ ,  $MedF(FAR_P^{MedM})$ ,  $MedF(FAR_{RH}^{MedM})$ , and  $MedF(FAR_W^{MedM})$ , respectively. Finally, we further identify the driver whose change plays an important role in the increasing fire risk via comparing the above our FARs over each region. At the global scale, we compared these four FARs via averaging these four separate FARs across selected regions. In addition, for each region, we also quantified uncertainties due to climate models and internal climate variability in these FARs based on the same standard deviation-based analysis applied for above  $FAR_{FWI}^n$ .

We tested that the approach above can provide insights into the relative contributions of the four drivers by inspecting whether  $MedF(FAR_{FWI}^{MedM})$  is similar to the sum of the separate FARs based on changes in the individual drivers. Specifically, we first aggregated the separate FARs from individual drivers for each fire extreme event introduced above ( $Sum(FAR_{driver}^n) = FAR_T^n + FAR_P^n + FAR_{RH}^n + FAR_W^n$ ). We then computed the multimodel median of  $Sum(FAR_{driver}^n)$  for each extreme fire event (hereinafter  $Sum(FAR_{driver})^{MedM}$  for simplicity) and then its median across events (hereinafter  $MedF(Sum(FAR_{driver})^{MedM})$ ). We found a high inter-regional correlation between the  $MedF(FAR_{FWI}^{MedM})$  defined above and  $MedF(Sum(FAR_{driver})^{MedM})$ , which supports the decomposition approach (Fig. S4c). Given that some differences in their absolute values exist, we further inspected the reasons for the difference. To this end, we computed a different counterfactual FWI by rescaling all drivers (P, T, RH, and W) to the counterfactual climate. Then, we used such a counterfactual FWI to compute the FAR for each extreme fire event  $n$ , referred to as  $FAR_{all\ drivers}^n$ , and successively derived the aggregated statistics  $MedF(FAR_{all\ drivers}^{MedM})$  as done for other FARs as described above (the median across fires of the multimodel median of FAR). Finally, we compared the difference between  $MedF(FAR_{all\ drivers}^{MedM})$  and  $MedF(FAR_{FWI}^{MedM})$ , which is similar to the above difference between  $MedF(Sum(FAR_{driver})^{MedM})$  and  $MedF(FAR_{FWI}^{MedM})$  (Fig. S4c, d)—this indicates that the difference between contribution from change in FWI itself and the sum of separate contributions from change in individual drivers arises mainly from the interaction among changes in individual drivers.

### The trend over time of human-induced climate change impact on fire extremes

For each region, to explore possible trends in the FAR across fires over time, we first derived the multimodel median of the  $FAR_{FWI}^n$  based on counterfactual FWI from different climate models for each extreme fire event  $n$ , that is  $FAR_{FWI}^{MedM}$ . Then, we quantified the trend in  $FAR_{FWI}^{MedM}$  by regressing it against the fire event occurrence date (the date of a weekly fire is defined as the third day of the week).

To quantify the change in FAR across years at the global scale, we derived yearly global FAR by first averaging the  $FAR_{FWI}^n$  across all fires of all selected regions for each year given one climate model and then obtaining the multimodel median. We finally quantified the linear trend in these multimodel median values over the years. To isolate the cause of such a trend, we quantified in the same fashion the trend over the years based on the four FARs from the change in individual drivers, that is the  $FAR_T^n$ ,  $FAR_P^n$ ,  $FAR_{RH}^n$ , and  $FAR_W^n$  introduced above. Finally, to ensure such a decomposition of  $FAR_{FWI}^n$  trend provides good insights, we also evaluated the trend over years in  $Sum(FAR_{driver}^n)$  and  $FAR_{all\ drivers}^n$ . In addition, to explain the change in these FARs over time, we further checked the change in FWI and individual FWI meteorological drivers across the years. To this end, we extended the analysis period (2001–2015) for scaling factors of FWI, T, P, RH, and W to the period 1901–2015. Specifically, we first calculated the regional spatial median of the scaling factors for each month. Then, given one climate model, we derived the yearly global scaling factor by computing the median of scaling factors across all months in the fire season of all selected regions in a given year (the median is preferred to the mean as it is less influenced by outliers). We finally obtained the multimodel median of such yearly scaling factors.

## Data availability

The daily burned area from GFED4 Database is available at <https://daac.ornl.gov/cgi-bin/dsviewer.pl?dsid=1293>. ERA5 daily meteorological data are available at <https://cds.climate.copernicus.eu/cdsapp#!/dataset/reanalysis-era5-single-levels?tab=overview>; CMIP6 data can be collected at <https://esgf-metagrid.cloud.dkrz.de/search>.

## Code availability

All computer codes used for the analyses are available from the authors upon request.

Received: 3 November 2024; Accepted: 23 March 2025;

Published online: 23 April 2025

## References

1. Lelieveld, J., Evans, J. S., Fnais, M., Giannadaki, D. & Pozzer, A. The contribution of outdoor air pollution sources to premature mortality on a global scale. *Nature* **525**, 367–371 (2015).
2. Burton, C. A. et al. Fire weakens land carbon sinks before 1.5 °C. *Nat. Geosci.* **17**, 1108–1114 (2024).
3. Park, C. Y. et al. Attributing human mortality from fire PM<sub>2.5</sub> to climate change. *Nat. Clim. Change* **14**, 1193–1200 (2024).
4. Curtis, P. G., Slay, C. M., Harris, N. L., Tyukavina, A. & Hansen, M. C. Classifying drivers of global forest loss. *Science* **361**, 1108–1111 (2018).
5. Kelly, L. T. et al. Fire and biodiversity in the anthropocene. *Science* **370**, eabb0355 (2020).
6. Van Der Werf, G. R. et al. Global fire emissions estimates during 1997–2016. *Earth Syst. Sci. Data* **9**, 697–720 (2017).
7. Andela, N. et al. A human-driven decline in global burned area. *Science* **356**, 1356–1362 (2017).
8. Jolly, W. M. et al. Climate-induced variations in global wildfire danger from 1979 to 2013. *Nat. Commun.* **6**, 7537 (2015).
9. Jain, P., Castellanos-Acuna, D., Coogan, S. C., Abatzoglou, J. T. & Flannigan, M. D. Observed increases in extreme fire weather driven by atmospheric humidity and temperature. *Nat. Clim. Change* **12**, 63–70 (2022).
10. Abatzoglou, J. T., Williams, A. P. & Barbero, R. Global emergence of anthropogenic climate change in fire weather indices. *Geophys. Res. Lett.* **46**, 326–336 (2019).
11. Barbero, R., Abatzoglou, J. T., Pimont, F., Ruffault, J. & Curt, T. Attributing increases in fire weather to anthropogenic climate change over France. *Front. Earth Sci.* **8**, 104 (2020).
12. Krikken, F., Lehner, F., Hausteine, K., Drobyshev, I. & van Oldenborgh, G. J. Attribution of the role of climate change in the forest fires in Sweden 2018. *Nat. Hazards Earth Syst. Sci.* **21**, 2169–2179 (2021).
13. Van Oldenborgh, G. J. et al. Attribution of the Australian bushfire risk to anthropogenic climate change. *Nat. Hazards Earth Syst. Sci.* **21**, 941–960 (2021).
14. Perkins-Kirkpatrick, S. E. et al. On the attribution of the impacts of extreme weather events to anthropogenic climate change. *Environ. Res. Lett.* **17**, 024009 (2022).
15. Touma, D., Stevenson, S., Lehner, F. & Coats, S. Human-driven greenhouse gas and aerosol emissions cause distinct regional impacts on extreme fire weather. *Nat. Commun.* **12**, 212 (2021).
16. Brown, P. T. et al. Climate warming increases extreme daily wildfire growth risk in California. *Nature* **621**, 760–766 (2023).
17. Abatzoglou, J. T. & Williams, A. P. Impact of anthropogenic climate change on wildfire across western US forests. *Proc. Natl Acad. Sci.* **113**, 11770–11775 (2016).
18. Burton, C. et al. Global burned area increasingly explained by climate change. *Nat. Clim. Change* **14**, 1186–1192 (2024).
19. Gillett, N., Weaver, A., Zwiers, F. & Flannigan, M. Detecting the effect of climate change on Canadian forest fires. *Geophys. Res. Lett.* **31**, 18 (2004).
20. Turco, M. et al. Anthropogenic climate change impacts exacerbate summer forest fires in California. *Proc. Natl Acad. Sci.* **120**, e2213815120 (2023).
21. Williams, A. P. et al. Observed impacts of anthropogenic climate change on wildfire in California. *Earth's Future* **7**, 892–910 (2019).
22. Shioyama, H. et al. Historical and future anthropogenic warming effects on droughts, fires and fire emissions of CO<sub>2</sub> and PM<sub>2.5</sub> in equatorial Asia when 2015-like El Niño events occur. *Earth Syst. Dyn.* **11**, 435–445 (2020).
23. Mengel, M., Treu, S., Lange, S. & Frieler, K. Attrici v1. 1-counterfactual climate for impact attribution. *Geoscientific Model Dev.* **14**, 5269–5284 (2021).
24. Randerson, J., Van Der Werf, G., Giglio, L., Collatz, G. & Kasibhatla, P. *Global Fire Emissions Database, Version 4.1 (gfedv4)*. (ORNL DAAC, 2015).
25. Hersbach, H. et al. The ERA5 global reanalysis. *Q. J. R. Meteorol. Soc.* **146**, 1999–2049 (2020).
26. Eyring, V. et al. Overview of the Coupled Model Intercomparison Project Phase 6 (CMIP6) experimental design and organization. *Geosci. Model Dev.* **9**, 1937–1958 (2016).
27. Fischer, E. M. & Knutti, R. Observed heavy precipitation increase confirms theory and early models. *Nat. Clim. Change* **6**, 986–991 (2016).
28. Bevacqua, E. et al. Direct and lagged climate change effects intensified the 2022 European drought. *Nat. Geosci.* **17**, 1100–1107 (2024).
29. Holden, Z. A., Morgan, P., Crimmins, M. A., Steinhilber, R. & Smith, A. M. Fire season precipitation variability influences fire extent and severity in a large southwestern wilderness area, United States. *Geophys. Res. Lett.* **34**, L16708 (2007).
30. Estes, B. L., Knapp, E. E., Skinner, C. N., Miller, J. D. & Preisler, H. K. Factors influencing fire severity under moderate burning conditions in the Klamath Mountains, northern California, USA. *Ecosphere* **8**, e01794 (2017).
31. Sullivan, A. L. Wildland surface fire spread modelling, 1990–2007. 2: Empirical and quasi-empirical models. *Int. J. Wildland Fire* **18**, 369–386 (2009).
32. Vicedo-Cabrera, A. M. et al. The footprint of human-induced climate change on heat-related deaths in the summer of 2022 in Switzerland. *Environ. Res. Lett.* **18**, 074037 (2023).
33. Bevacqua, E. et al. More meteorological events that drive compound coastal flooding are projected under climate change. *Commun. Earth Environ.* **1**, 47 (2020).
34. Calvin, K. et al. IPCC 2023: Climate change 2023: Synthesis report. *Contribution of Working Groups I, II and III to the Sixth Assessment Report of the Intergovernmental Panel on Climate Change*. 1–34 (IPCC, 2023).
35. Wang, Y. & Huang, P. Potential fire risks in South America under anthropogenic forcing hidden by the Atlantic Multidecadal Oscillation. *Nat. Commun.* **13**, 2437 (2022).
36. Kirchmeier-Young, M. C., Gillett, N. P., Zwiers, F. W., Cannon, A. J. & Anslow, F. Attribution of the influence of human-induced climate change on an extreme fire season. *Earth's Future* **7**, 2–10 (2019).
37. Wagner, C. V. *Development and Structure of the Canadian Forest Fire Weather Index System*. Canadian Forestry Service, Headquarters, Ottawa. Forestry Technical Report 35. 35 p (1987).
38. Mitchell, D. et al. Half a degree additional warming, prognosis and projected impacts (HAPPI): background and experimental design. *Geosci. Model Dev.* **10**, 571–583 (2017).
39. Maraun, D. et al. A severe landslide event in the Alpine foreland under possible future climate and land-use changes. *Commun. Earth Environ.* **3**, 87 (2022).
40. Jézéquel, A. et al. Conditional and residual trends of singular hot days in Europe. *Environ. Res. Lett.* **15**, 064018 (2020).
41. Ramos, A. M. et al. The compound event that triggered the destructive fires of October 2017 in Portugal. *iScience* **26**, 106141 (2023).

42. Shen, C. et al. Evaluation of global terrestrial near-surface wind speed simulated by cmip6 models and their future projections. *Ann. N. Y. Acad. Sci.* **1518**, 249–263 (2022).
43. Simpson, I. R. et al. Observed humidity trends in dry regions contradict climate models. *Proc. Natl Acad. Sci.* **121**, e2302480120 (2024).
44. Donat, M. G. et al. How credibly do cmip6 simulations capture historical mean and extreme precipitation changes? *Geophys. Res. Lett.* **50**, e2022GL102466 (2023).
45. Deser, C., Knutti, R., Solomon, S. & Phillips, A. S. Communication of the role of natural variability in future North American climate. *Nat. Clim. Change* **2**, 775–779 (2012).
46. Ribeiro, A. F. et al. The time since land-use transition drives changes in fire activity in the Amazon-Cerrado region. *Commun. Earth Environ.* **5**, 96 (2024).
47. Chen, Y. et al. Multi-decadal trends and variability in burned area from the 5th version of the Global Fire Emissions Database (gfed5). *Earth Syst. Sci. Data* **15**, 5227–5259 (2023).
48. Vitolo, C., Di Giuseppe, F., Krzeminski, B. & San-Miguel-Ayanz, J. A 1980–2018 global fire danger re-analysis dataset for the Canadian Fire Weather Indices. *Sci. Data* **6**, 1–10 (2019).
49. Vitolo, C. et al. ERA5-based global meteorological wildfire danger maps. *Sci. Data* **7**, 216 (2020).
50. Quilcaille, Y., Batibeniz, F., Ribeiro, A. F., Padrón, R. S. & Seneviratne, S. I. Fire weather index data under historical and shared socioeconomic pathway projections in the 6th phase of the Coupled Model Intercomparison Project from 1850 to 2100. *Earth Syst. Sci. Data* **15**, 2153–2177 (2023).
51. Agency, I. E. *World Energy Outlook* (OECD/IEA Paris, 2009).
52. Iturbide, M. et al. An update of IPCC climate reference regions for subcontinental analysis of climate model data: definition and aggregated datasets. *Earth Syst. Sci. Data* **12**, 2959–2970 (2020).
53. Richards, J., Huser, R., Bevacqua, E. & Zscheischler, J. Insights into the drivers and spatiotemporal trends of extreme mediterranean wildfires with statistical deep learning. *Artif. Intell. Earth Syst.* **2**, e220095 (2023).
54. Kirchmeier-Young, M. C. et al. Human driven climate change increased the likelihood of the 2023 record area burned in Canada. *npj Clim. Atmos. Sci.* **7**, 316 (2024).
55. Park, I. W., Mann, M. L., Flint, L. E., Flint, A. L. & Moritz, M. Relationships of climate, human activity, and fire history to spatiotemporal variation in annual fire probability across California. *PLoS ONE* **16**, e0254723 (2021).

## Acknowledgements

S.F. acknowledges the support provided by the China Scholarship Council (CSC). E.B. and this project received funding from the Deutsche

Forschungsgemeinschaft (DFG, German Research Foundation) via the Emmy Noether Programme (grant ID: 524780515). This project has received funding from the European Union's Horizon 2020 research and innovation programme under grant agreement No 101003469 (XAIDA). We thank Andreia FS Ribeiro for insightful discussions.

## Author contributions

S.F. and E.B. initiated the study and designed the research; E.B. supervised the project; S.F. performed all analyses and created all figures; S.F. and E.B. wrote the paper; all authors contributed to the interpretation of the results and edited the manuscript.

## Funding

Open Access funding enabled and organized by Projekt DEAL.

## Competing interests

The authors declare no competing interests.

## Additional information

**Supplementary information** The online version contains supplementary material available at <https://doi.org/10.1038/s41612-025-01021-z>.

**Correspondence** and requests for materials should be addressed to Sifang Feng or Emanuele Bevacqua.

**Reprints and permissions information** is available at <http://www.nature.com/reprints>

**Publisher's note** Springer Nature remains neutral with regard to jurisdictional claims in published maps and institutional affiliations.

**Open Access** This article is licensed under a Creative Commons Attribution 4.0 International License, which permits use, sharing, adaptation, distribution and reproduction in any medium or format, as long as you give appropriate credit to the original author(s) and the source, provide a link to the Creative Commons licence, and indicate if changes were made. The images or other third party material in this article are included in the article's Creative Commons licence, unless indicated otherwise in a credit line to the material. If material is not included in the article's Creative Commons licence and your intended use is not permitted by statutory regulation or exceeds the permitted use, you will need to obtain permission directly from the copyright holder. To view a copy of this licence, visit <http://creativecommons.org/licenses/by/4.0/>.

© The Author(s) 2025